Journal of Materials Chemistry A

Accepted Manuscript

ROYAL SOCIETY OF CHEMISTRY

www.rsc.org/materialsA

Journal of Materials Chemistry A

PAPER

Highly efficient and durable dye-sensitized solar cell based on wet-laid PET membrane electrolyte

Received 00th January 20xx,
Accepted 00th January 20xx

DOI: 10.1039/x0xx00000x
www.rsc.org/MaterialsA

Kyung Chul Sun [1,2+], Iftikhar Ali Sahito [3+], Jung Woo Noh[1], Sang Young Yeo[1], Jung Nam Im[1], Sung Chul Yi[2,4], Yeon Sang Kim[1*], Sung Hoon Jeong[3*]

Poly ethylene terephthalate (PET), a commonly used textile fiber, was used in the form of a wet-laid nonwoven fabric as a matrix for an electrolyte in dye-sensitized solar cells (DSSCs). Also functioning as a separator between the photoanode and cathode of a DSSC, this nonwoven membrane was prepared by a well-known wet-laid manufacturing process followed by calendaring to reduce the thickness and increase uniformity in structure. This membrane can better absorb electrolyte turning into a quasi-solid, providing excellent interfacial contact between both electrodes of the DSSC and preventing a short circuit. An optimized membrane provides better and more desirable structure for ionic conductivity, resulting in the improvement of the photovoltaic performance after calendaring. The quasi-solid-state DSSC assembled with an optimized membrane exhibited 10.248% power conversion efficiency (PCE) at 100 mW/cm². With the aim of increasing the absorbance, the membrane was also plasma-treated with argon and oxygen separately, which resulted in retention of the electrolyte, avoiding its evaporation, and a 15% longer lifetime of the DSSC compared to liquid electrolyte. The morphology of the membrane was studied by field emission scanning electron microscopy, and the photovoltaic properties and impedance spectroscopy of the cells were studied using polarization curves and electrochemical impedance spectroscopy, respectively. The results suggest that this novel membrane can be used in high-efficiency solar cells, increasing their lifetime without compromising the photovoltaic properties.

1. Introduction

Textiles being low-cost, lightweight, flexible, and easily fabricated with a large amount of verities, have gained tremendous attention recently for their use in energy harvesting [1-5]. Non-woven fabrics, in the form of thin membranes, provide high porosity, resulting in the absorption of more aqueous solution. On the other hand, the wet-laid process for producing non-woven fabrics have gained much interest because of the ease of processing and scalability of production[6]. Non-woven fabric produced in this way can be used as a separator because it does not conduct electricity intrinsically; however, owing to its high absorbance, it can have high ionic conductivity, allowing the rapid transport of ions required for a high-efficiency electrolyte in dye-sensitized solar cells (DSSCs)[7]. Another advantage of using such materials is their flexibility, which makes them suitable for use in flexible solar cell applications. Commonly used polyethylene terephthalate (PET) is a cheap and strong synthetic fiber which is used for a variety of applications ranging from apparel to technical[8, 9] and is also used in medical applications[10, 11]. Owing to its low cost and availability in various forms, coupled with resistance to strong chemicals, non-woven PET fabric can be manufactured in a variety of styles and shapes.

DSSCs have been focused on as a promising alternative to conventional solar cells due to their low cost, ease of fabrication, and suitability for a wide variety of applications[12, 13]. However, DSSCs prepared by sealing the liquid electrolyte between the photo anode and cathode suffer from the problem of electrolyte evaporation, which reduces the efficiency of the cell[14-17]. Even highly efficient cells prepared with liquid electrolyte sealed inside do not prove to be durable long term; therefore, researchers are trying to use other forms of electrolytes that could provide cells with better resistance to weathering effects with less evaporation of the electrolyte, including non-volatile ionic liquids[18, 19], polymer-based gel electrolytes[20-24] and solid electrolytes[25, 26]. Ionic liquid electrolytes have much lower efficiency, and the injection of a gel-based electrolyte is also a difficult step, due to its high viscosity; therefore, the efficiency of the DSSC falls far below that of those prepared with a liquid electrolyte. In such a case, the high ionic conductivity and high absorbance of the

[1]Research Institute of Industrial Technology Convergence Technical Textile and Materials R&D Group, Korea Institute of Industrial Technology
[2]Department of Fuel cells and Hydrogen Technology, Hanyang University
[3]Department of Organic and Nano Engineering, Hanyang University
[4]Department of Chemical Engineering, Hanyang University
[+] These authors have equal contribution.
*Corresponding authors. +82 2 2220 0498

E-mail address: yskim@kitech.re.kr (Yeon Sang Kim), shjeong@hanyang.ac.kr (Sung Hoon Jeong).

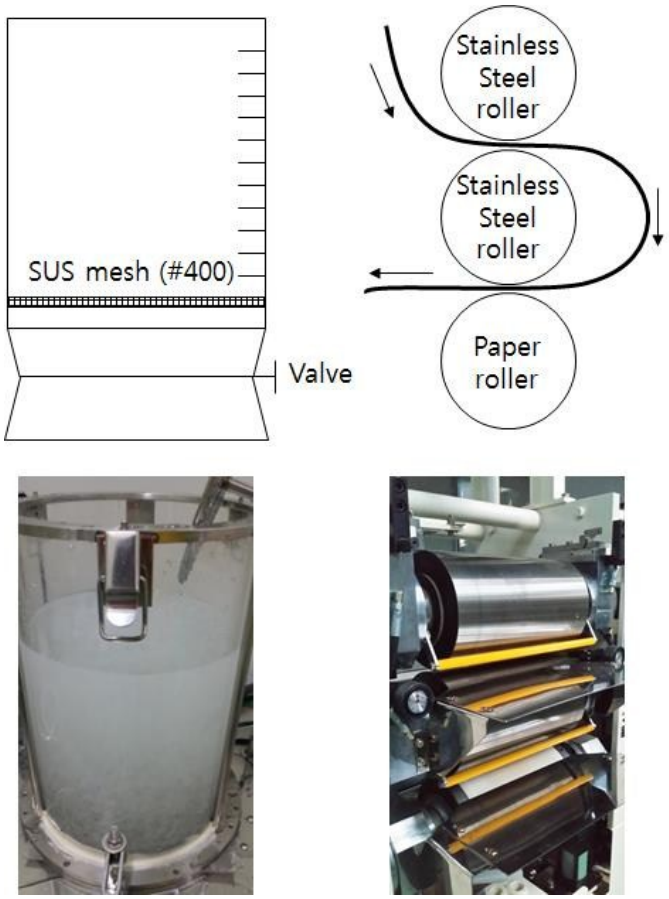

Figure 1. Schematic illustration of lab-scale wet-laid system (top left), an actual photograph of it (bottom left), calendaring machine (top right) and actual machine (right bottom).

electrolyte together with resistance to the solvents used in the electrolyte are crucial properties for this type of separator. Recently, a very high conversion efficiency of 14.3%[27] has been achieved in a DSSC based on a liquid electrolyte; however, its lifetime is unknown. To address these issues, electrolytes based on membrane can be the best option for the fabrication of flexible, efficient and durable devices. Bella et al[28] prepared crosslinked polymer electrolyte membrane and modified with Titanium mesh (TiO_2 nanotubes grown) to fabricate a flexible DSSC, however, the efficiency of the cells was only 3.4%. Gerbaldi et al[29] studied and compared the effect of carboxymethyl cellulose and micro-fibrillated cellulose as bio-sourced filler in quasi-solid electrolyte for polymeric membrane based DSSCs. However, the preparation of membrane was time consuming, due to complex synthesis method and polymerization, and the fill factor of the cell was also very low.

Herein, we report a novel, thin, nonwoven porous PET textile, which is capable of absorbing more electrolyte. It also shows improved durability due to its high ionic transport properties in conjunction with better solar cell durability with high photovoltaic efficiency, which is as good as that of a liquid electrolyte. Other advantages include ease of processing, low cost, and flexibility as well as quicker and scalable fabrication. To improve the evenness of the produced nonwoven fabric, it was calendared, and to improve the absorbance, the layer was

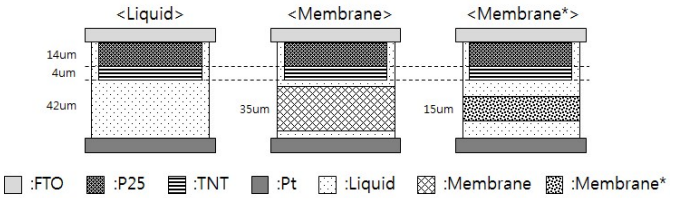

Figure 2. Schematic layout of DSSCs with various structures (Membrane*= after calendaring sample)

plasma-treated with argon and oxygen separately. The results were compared with those obtained with a conventional liquid electrolyte in terms of photovoltaic and electrochemical properties, and the lifetimes of the cells were also compared. The resulting DSSCs were optimized, and they exhibited a high photovoltaic conversion efficiency (PCE) of more than 10% at 1 Sun illumination and a longer lifetime

2. Experimental

2.1 Materials

For the synthesis of titania nanotubes (TNTs), TiO_2 (P25 by Degussa Co.), NaOH (98%, Samchun Co.), Hydrochloric acid (37%, Samchun Chemicals Co.) and DI water were used. For the preparation of TiO_2 pastes for photoelectrodes; P25 (Degussa Co.) and TNT, ethyl cellulous (Sigma-Aldrich Co.), terpineol (Aldrich Co.), and acetic acid (99.7%, Junsei Co.) were used as received. For fabrication of the wet-laid-based PET nonwoven fabric, PET short-cut (0.06, 0.4, 1.1 De composite, 5 micrometers, Clean and Science Co.), a dispersing agent (Triton X-100), an antifoaming agent (polydimethylsiloxane), and adhesives (polyacrylamide and poly ethylene oxide composite, Clean and Science Co.) were used. For the photovoltaic cell assembly, FTO glass (TEC 7, Pilkington Co.), N719 (cis-diisothiocyanato-bis (2,2'-bipyridyl-4,4'-dicarboxylato) ruthenium (II) bis (tetrabutylammonium), Solaronix Co.), Surlyn for spacers (60 um, Dupont Co.) and an anti-reflecting film (AR film, Toray chem. Co.) were used as received. Also, 1-butyl-3-methylimidazolium iodide (BMII, Merck Co.), iodine (I_2, Merck Co.), lithium iodine (LiI, Sigma-Aldrich Co.), 4-tert-butylpyridine (TBP, Sigma-Aldrich Co.), and anhydrous acetonitrile were purchased for the preparation of electrolytes.

2.2 Wet-laid process for PET non-woven membrane

The PET-based membrane was prepared using the wet-laid method as mentioned in previous literature[30-32]. PET staple fibers of 0.2 wt: % (1.0g) were placed in a PTFE-covered vessel containing 500 mL of H_2O. A dispersing agent (1.0 mg) and an antifoaming agent (1.0 mg) were mixed with the PET staple fibers, which were dispersed in solution under stirring at 4,400 rpm for 10 min. After stirring, 7,500 mL of H_2O and adhesives (0.3 mg) were added to the vessel under continuous stirring at 4,400 rpm for 10 min. After that, the prepared slurry was removed from the vessel and then transferred to a lab-scale wet-laid system (Fig. 1). The PET particles were allowed to rest, and the supernatant was removed from the wet-laid system. Then, the mixed precursor was placed on a stainless steel (SUS) mesh indiscriminately. After drying below 70 °C for 4 h, a highly uniform PET-based nonwoven membrane was produced. To

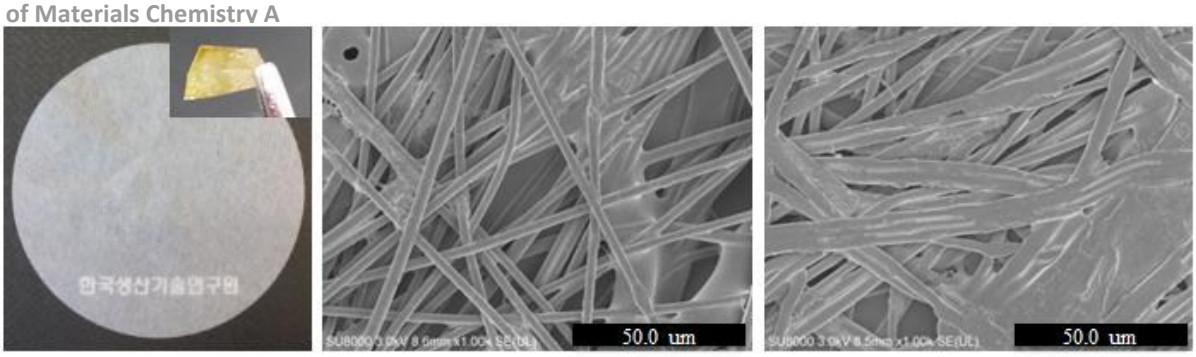

Figure 3. Original image of the prepared nonwoven membrane and electrolyte-immersed membrane (left and left-inner) and FE-SEM images (x 1,000) of a wet-laid PET membrane (centre) and a hot-pressed membrane (right)

reduce the thickness and improve the uniformity in terms of pore size and volume, the nonwoven fabric was calendared (pressed between cylinders) three times under 60 kg/cm^2 of pressure at 180 °C. Furthermore, to increase the absorbance of the liquid electrolyte, the prepared membrane was treated by oxygen and argon plasma separately for 2 min at 100 W using a plasma chamber (Europlasma Co., Italy).

2.3 Photo anode preparation

For the fabrication of highly efficient photo anodes using TNT as an over layer, the recipe was used from our previous work[33, 34]. FTO glasses were cleaned with acetone, DI water, and ethanol by sonication and then dried. The cleaned FTO glasses (15×15 mm^2) were immersed in $TiCl_4$ solution (40 mM in water) for 30 min at 70 °C and successively washed with water and ethanol. After washing, the FTO substrates were annealed at 500 °C for 30 min. The pre-treated FTO glasses were coated with a DMT structure using a doctor blade [35]. After printing of the main layer, the TiO_2 films were heated in six steps of 70 °C, 125 °C, 325 °C, 375 °C, 450 °C, and 500°C for 30, 30, 5, 5, 15, and 15 min, respectively, using a high temperature furnace (Lab House Co.). The active area of the cells was about 4×5 mm^2, which was measured by using a software equipped Camscope (ICS-305B, Sometech Co.). For post-treatment, the coated and sintered TiO_2 films were immersed in $TiCl_4$ solution (40 mM in water) for 30 min at 70 °C. After washing with water and ethanol, the films were again annealed at 500 °C for 30 min. After cooling down to less than 80 °C in a furnace, the annealed TiO_2 films were rapidly immersed in N719 solution (0.5 mM in ethanol) and kept in an airtight glass-container at room temperature under dark and dry conditions for 24 hours.

2.4 DSSC assembly

The dye-covered photo anodes were washed to remove any unfixed dye using ethanol and then dried under nitrogen flow. The photo anodes and Pt-electrodes were sandwiched together using ionomer spacer by hot-pressing at 80 °C for 20 sec. After pressing, the electrolyte solution was injected into the cells through the one-holed FTO glass by capillary effect under vacuum, and the holes were sealed with cover-glasses using the same spacer. The PET-membrane-based DSSCs were fabricated by sandwiching a slice of the separator membrane between the photo anode and the Pt-electrode. The schematic diagram in Fig. 2 shows the cells with different structures containing assemblies with different electrolyte types. Membrane and inner-spacer size is 6x10 mm^2. The resulting cells had an illuminated area of 0.2 cm^2 with AR film and black masking.

2.5 Measurements

The morphology and structure of the materials were investigated by field emission-scanning electron microscopy (FE-SEM, JEOL JSM-6700F). Load tests were measured using UTM with 150 N loader. Pore size and porosity were measured using AUTOPORE V through Mercury porosimetery (Micromeritics Co.) and CFP-1200-AEL through a capillary flow porometer (PMI Co.). Photocurrent-voltage measurement was performed using a K101-Lab20 (Mac Science Co.) source measuring unit. A solar simulator with a 160 W Xenon arc lamp was used as a light source satisfying AAA class (spectral match; 0.75~1.25, non-uniformity of irradiance; ≤±2%, temporal instability; ≤±2%). The light intensity was calibrated with a KIER-calibrated Si solar cell (Mc Science Co.). The electrochemical impedance spectra of the full cells were measured using ultimate electrochemical workstation in the frequency range of 0.05 Hz to 500 kHz under 100 m W/cm^2 (BioLogic Co.). The ionic conductivity of the membrane was measured by electrochemical impedance spectroscopy (EIS) at room temperature using the symmetrical cells method[36]. The electrolyte resistance, R, was measured using ultimate electrochemical workstation in the frequency range of 0.1 Hz to 100 kHz, the AC oscillation was 10 mV. The diffusion constant of I_3^- was determined by the same electrochemical workstation and the symmetric cells of a cyclic voltammogram using a slow scan rate (scan rate: 5 mV/s, potential: -1 to 1 V). Their active area was 0.6 cm^2.

3. Results and Discussion

Table 1. Porosity and pore size of prepared PET membrane

	Total intrusion Volume (mL/g)	Total pore area (m^2/g)	Apparent density (g/mL)	Porosity (%)	Smallest pore (μm)	Mean flow pore (μm)	Bubble point pore (μm)	Standard deviation
Bare	6.7925	13.490	0.6975	82.5706	34.3064	483.3546	666.0178	443.4995
Calendared	5.1979	11.373	0.7859	80.3344	17.6756	32.6043	663.9853	137.2946

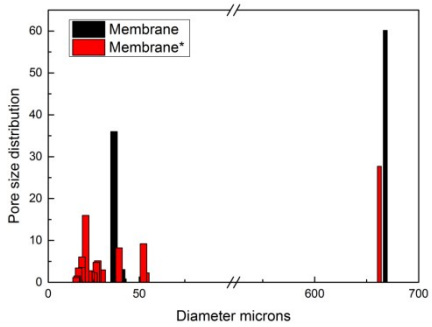

Figure 4. Pore-size distribution

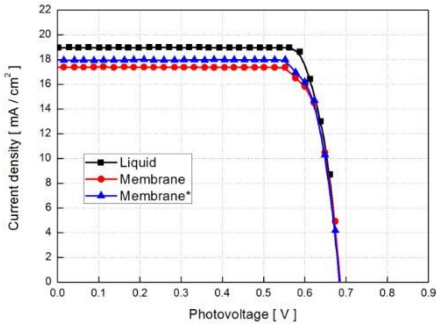

Figure 5. Polarization curves of DSSCs with various electrolytes under simulated AM 1.5 global sunlight (1 Sun, 100 mW/cm^2)

3.1 Characterization of Wet-laid PET membrane

Fig. 3 shows SEM images of the prepared PET membrane consisting of fibers as a web with an average diameter of about 2.5 µm. This membrane had high porosity and a completely interconnected-3D network structure. After calendaring, the pore size was decreased, resulting in better uptake of the electrolyte due to an even sheet thickness and improved distribution of the pores. The Bare and calendared membranes show increased adequate strength to handle the membrane with ease. Bare membrane showed maximum load of 271.1 and the calendared one showed 350.7 gf. The tensile stress at maximum load was found 39.9 and 159.4 kgf/cm^2 with elongation at maximum load of 22.1 and 23.2 % respectively. The pore size and porosity percentage of the bare and calendared membranes were measured and are listed in Table 1. The bare membrane had a porosity of 82.57% which was slightly decreased to 80.33% after the calendaring, whereas the total pore area reduced from 13.49 m^2/g to 11.37 m^2/g. However, after calendaring, the smallest pore size of 17.67 µm in the calendared sample was closer to the mean flow pore of 32.60, whereas in the bare sample, the difference between the smallest pore size and the mean flow pore was much higher, indicating that calendaring caused the samples to have a higher uniformity with respect to properties that can be attained, resulting in more regular transport of ions inside the membrane. The pore size distribution of the nonwoven membranes before and after calendaring is plotted in Fig. 4. The bubble point pore in the bare membrane is 666.0178 µm, which is too wide to be called a pore, instead it can be considered a hole. As seen in the distribution graph, around 60% of the pores fall in this category, and as listed in Table 1, the average pore size for the bare membrane is 483.3546 µm. Such a large pore may be regarded as a defect, and may not retain the electrolyte for long. However, as seen in Table 1, after calendaring, the average pore size dropped to only 32 µm. Also as seen in Fig. 3, only 25% of the pores fall near the bubble point pore, making the membrane more uniform with respect to pore size. With small and more uniformly distributed pores, the electrolyte can be easily held inside the membrane for a longer period of time and the membrane may be able to hold sufficient electrolyte for longer. It is also important to note that, after calendaring, the contact between the fibers constructing the membrane increases, thereby resulting in better transport of the electrolyte ions through newly formed channels.

Table 3. Photovoltaic performance of DSSCs with various electrolytes (membrane* = after calendaring sample)

Electrolyte type	V_{OC} [V]	J_{SC} [mA]	FF [%]	PCE [%]
Liquid	0.686	18.958	85.937	11.176
Membrane	0.689	17.370	82.996	9.933
Membrane*	0.686	17.955	83.145	10.241

Nine (09) membranes were randomly chosen and measured for thickness before and after calendaring. Their calculated weight and statistical analysis results are given in Table 2. The average thickness of the bare samples was measured as 35.3 µm, which dropped to only 14.9 µm after calendaring. It was observed that calendared samples had less variation and showed smaller standard deviation (STD) and coefficient of variation (CV%) values compared to non-calendared samples, as shown in the Table 2. This can be ascribed to the uniformity of the membrane which is required for high-efficiency cells because of better ionic transport due to a more compact structure.

3.2 Photovoltaic performance of the DSSCs

Fig. 5 shows the overall photovoltaic performance, current-voltage (J-V curve), of the DSSCs prepared using bare, calendared non-woven membrane electrolyte and the liquid electrolyte, evaluated under AM 1.5 illumination (1 sun, 100 mW/cm^2). The obtained cell parameters of the short-circuit current (J_{SC}), open-circuit voltage (V_{OC}), fill factor (FF), and overall conversion efficiency (PCE%) are summarized in Table 3. Figure 5 and Table 3 show that the liquid-electrolyte-based cells achieved better photovoltaic performance than both types of non-woven samples. The overall conversion of the liquid-electrolyte-based cell was 11.18% compared to 9.93% and

Table 2. Thickness of prepared PET membrane before and after calendaring with statistical analysis [all units are in µm]

Sample	1	2	3	4	5	6	7	8	9	Range	AVG	STD	CV%
Bare	31	33	35	36	34	36	40	38	35	9	35.3	2.4	7.1
Calendared	14	15	14	15	16	16	16	14	14	2	14.9	0.9	5.9

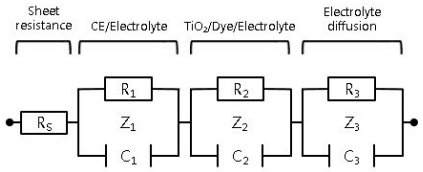

Figure 6. Equivalent circuit of the cell comprising a substrate, electrolyte, and porous structured electrode

10.24%, showed by the bare and calendared membrane-based cells, respectively. The J_{SC} of the liquid-electrolyte-based cell of 18.95 mA/cm² was higher than those of 17.37 mA/cm² and 17.95 mA/cm² of the bare and calendared membrane-based cells, respectively. Additionally, there was not much difference between the V_{OC} of the three cells, which can be attributed to the excellent interfacial contact between the two electrodes and high ionic transport, even when the proposed nonwoven fabric was used. It was also revealed that the bare membrane reached 88.9% of the performance of liquid, and the calendared nonwoven membrane reached 91.6%, suggesting that this novel thin, wet-laid, nonwoven membrane can certainly be used as an electrolyte medium in high-performance DSSCs.

3.3 Electrochemical properties of the DSSCs

The internal kinetics of DSSCs, such as the essence of hole-electron transport processes and the behaviours of interfacial charge transport, can be understood by measuring the electrochemical impedance spectra (EIS) of solar devices[37-39]. All the EIS spectra were simulated using EC-Lab software according to the equivalent circuit shown in Fig. 6. The internal resistance and capacitance values of the cells are listed in Table 4, and the corresponding Nyquist plots are shown in Figure 7. In a Nyquist plot, the complex impedance of a typical DSSC is the sum of all components, given as R_S, Z_1, Z_2, and Z_3. Here, R_S denotes the contact impedance between the substrate (FTO) and metal ohmic contact (series resistance, R_S), which is the only real part of impedance. The first semicircle corresponds to the charge transfer resistance at the counter electrode to electrolyte interface. The second semicircle shows complex impedance of the interface among the photo anode, dye molecules, and the redox shuttle. The final semicircle represents the diffusion of tri-iodide ions related to the Warburg impedance; it can also be hidden in second semi-circle.

As shown in the Nyquist plots in Fig. 7, the starting point of the EIS, which is R_S is same, as that of the electrode in all three cases is the same FTO glass. However, as the first semicircle is build up, the distinction starts to reveal, as the liquid-electrolyte-based cells provide less interfacial resistance and lower impedance than the other two cells. The membrane-based cells show a slightly higher impedance trend due to the contact between the membrane and the counter electrode. This contact

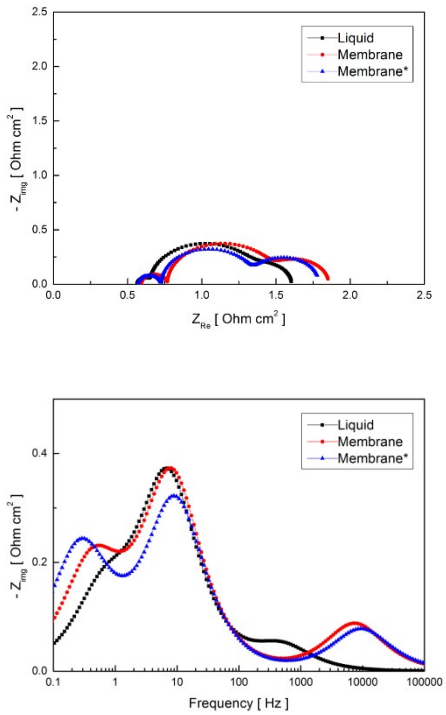

Figure 7. Electrochemical analysis (EIS) of the DSSC's based on various electrolyte structures under full illumination (above; Nyquist plot and below; Bode plot)

can make lower active area of the substrate, thereby decreasing the ionic transport and electron transfer in the cells. The structure having membrane shows larger second semi-circle due to the higher interfacial charge resistance between the semiconductor and redox shuttle. However, the calendared, thin membrane showed a relatively shorter semicircle than the thicker one, owing to its better evenness. Hence, it can be concluded internal resistance depends upon the thickness, as we know that resistance = (thickness) / (area).

The charge transport and conductivity behaviour of the DSSCs can be explained by the Nyquist plots shown in Fig. 7 (top). It can be seen that the liquid-electrolyte-based cells show higher total impedance shifted towards left, thereby indicating a lower recombination rate than that of the nonwoven-membrane-based electrolyte. However, between the other two, the calendared, thin non-woven-membrane-based cells showed a higher peak due to the lower recombination rate compared to that of the bare membrane.

The electron life time (τ_e) is obtained from the Bode plot peaks in the middle-frequency range (0.1 to 100 Hz), by following relation[30] in which 'f' is the frequency of peak.

$$\tau_e = \frac{1}{\omega} = \frac{1}{2\pi f}$$

Table 4. EIS internal resistance of DSSCs including liquid and non-woven membrane-based electrolytes

Electrolyte type	R_S [Ohm cm²]	R_1 [Ohm cm²]	C_1 [F cm⁻²]	R_2 [Ohm cm²]	C_2 [F cm⁻²]	R_3 [Ohm cm²]	C_3 [F cm⁻²]	τ_e [ms]	δ [S/cm]	$D_{I_3^-}$ [cm²/s]
Liquid	0.566	0.088	3.59e-03	0.697	3.19e-02	0.255	1.000	23.49	0.0209	3.64e-06
Membrane	0.593	0.175	1.21e-04	0.706	2.73e-02	0.386	9.89e-01	21.37	0.0036	1.43e-06
Membrane*	0.570	0.155	1.08e-04	0.617	2.77e-02	0.450	1.291	17.76	0.0137	1.65e-06

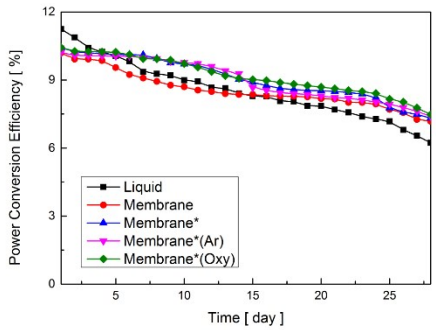

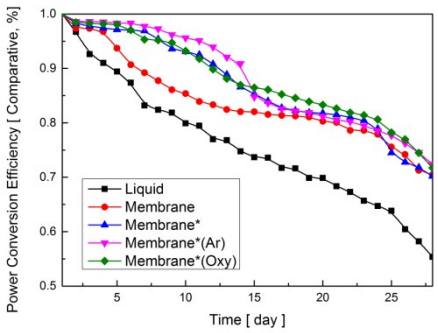

Figure 8. Variation of power conversion efficiency as a function of time for DSSCs

It is not clear significantly that for all the sets having various electrolyte structure, the effective electron life time for prepared cells are almost similar, frequency difference of 1 or 2 steps. Therefore, we focused on different ionic conductivities and diffusion coefficient of electrolyte.

Table 4 lists the ionic conductivities (**δ**) and diffusion coefficient of I_3^- ($D_{I_3^-}$) of the three different types of electrolytes (The bulk resistance of symmetrical cells and cyclic voltammogram plots were shown in supporting information Fig S2 and S3). The liquid electrolyte, as a reference, exhibits an ionic conductivity of 2.09 × 10^{-2} S cm^{-1} at room temperature; whereas the bare and calendared non-woven show ionic conductivities of 0.36 × 10^{-2} S cm^{-1} and 1.37 × 10^{-2} S cm^{-1}, respectively. There was no boundary separation between electrolyte and electrode. The decrease in the ionic conductivity and diffusion coefficient with the bare membrane is related to the generation of free volume at the membrane interface[40]. The pressed membrane having decreased porosity and pore size with increased evenness showed better ionic conductivity and diffusion coefficient. These results indicate that the pressed membrane provides the most desirable structure for ionic transport among the electrolytes under study. In comparison with the results of photocurrent and diffusion coefficient of I_3^-, an increase in J_{SC} with types of membrane is related to improved diffusion of I_3^-, as shown in Tables 3 and 4. On the other hand, the type of electrolyte has only a minor influence on the V_{OC}, indicating the nonwoven membrane works as well as the liquid electrolyte.

3.4 Long-term stability of DSSCs with plasma-treated membrane

In addition to the high photovoltaic properties, the long-term stability of cells is a very important parameter of DSSC, and better absorption of electrolyte in the separator can enhance the life of the cells[35]. As mentioned earlier, the calendared PET membranes were plasma-treated with argon and oxygen separately for higher absorption of the electrolyte, aiming to retain most of the electrolyte and maintain a higher long-term stability, were also compared with other types of electrolytes in terms of long-term durability of the DSSCs. The PCE values of the cells were recorded at regular intervals for four (04) weeks as a function of time, and the results are plotted in Fig. 8. In order to expedite the effect of atmospheric conditions, the cells were kept at 60℃ [41].

Though the DSSC assembled with liquid electrolyte showed high efficiency after being assembled, its PCE decreased continuously during the testing period. The cell lost 45% of its initial conversion efficiency after 4 weeks. The normal decay of PCE in the DSSC based on liquid electrolyte is related to the evaporation of the electrolyte due to imperfect sealing of the DSSC having a thinner nanostructure. The bare PET-based DSSC lost PCE rapidly within 2 weeks; however, it remained almost constant until 3 weeks. The overall drop in the PCE of the bare-PET-based DSSC was 30%, which was much lower than that of the liquid-electrolyte-based cells. On the other hand, the calendared-PET-based DSSC lost PCE slower than the bare-PET cell; however, after 24 days, it lost PCE rapidly and showed similar PCE loss as of bare-PET cells. Of the plasma-treated samples, the argon-treated sample showed slightly higher efficiency compared to oxygen treated one. The oxygen plasma can be said to have better effect on the uptake, yet it may also deteriorate the surface of PET substrate [42], due to which, the cells may have shown a slightly lower efficiency in the first 15 days. The argon plasma, as is less effective on the organic impurities, which may have remained on the substrate and in contact with the electrolyte may have started to react with argon to lessen its effect which might be the reason of drop in efficiency after 15 days. Though the exact reasons are not known, therefore, we propose this investigation as a future work. These results clearly indicate that plasma treatment increases the cell lifetime of membrane-based DSSCs. To support the discussion, we conducted the wicking test for the four types of the membranes used in the experiment. The membranes were dipped in the electrolyte solution and the results were recoded after 100 sec in order to allow the membranes to complete the possible wicking inside their pores. As shown in Fig S5, the plasma treated membranes resulted with higher uptake of the electrolyte compared to non-treated. However, there no significant difference in the uptake of oxygen and argon plasma treated samples.

4. Conclusion and future suggestions

In conclusion, a thin, lightweight, low-cost and easily fabricated PET nonwoven membrane was successfully synthesized through a scalable wait-laid process, commonly known in the non-woven textile industry. This novel membrane was used as a matrix for liquid electrolyte with high absorbance. The optimized DSSC assembled with a calendared membrane exhibited a very high PCE of 10.24%, reaching 91.74% of reference cell value, giving better long-term stability compared

to the reference liquid-electrolyte-based DSSC under 1 Sun illumination. In addition, the nonwoven membrane was plasma-treated to enhance its uptake towards the electrolyte to increase the long-term stability of the DSSC, which resulted in a 15% longer lifetime compared to the liquid-electrolyte-based DSSC. The ionic transport and diffusion coefficients of the membrane-based cells were almost the same as those of the liquid electrolyte, demonstrating its suitability for use in high efficiency DSSC. If possible to prepare more thinner membrane without calendaring process, it can be provide more useful information for this study. The proposed novel membrane is a promising candidate to further improve the lifetime and efficiency of electronic devices, and it will provide a useful step towards the development of next-generation photovoltaics.

Acknowledgements

This work was supported by the ministry of trade, industry and energy, Republic of Korea (10049639) and a Manpower Development Program for Energy, supported by the Ministry of Knowledge Economy (MKE), Republic of Korea.

References

1. Y. J. Yun, W. G. Hong, W.-J. Kim, Y. Jun and B. H. Kim, *Advanced Materials*, 2013, **25**, 5701-5705.
2. G. Yu, L. Hu, M. Vosgueritchian, H. Wang, X. Xie, J. R. McDonough, X. Cui, Y. Cui and Z. Bao, *Nano letters*, 2011, **11**, 2905-2911.
3. Y. A. Samad, Y. Li, S. M. Alhassan and K. Liao, *RSC Advances*, 2014, **4**, 16935.
4. I. A. Sahito, K. C. Sun, A. A. Arbab, M. B. Qadir and S. H. Jeong, *Electrochimica Acta*, 2015, **173**, 164-171.
5. A. A. Arbab, K. C. Sun, I. A. Sahito, M. B. Qadir and S. H. Jeong, *Physical Chemistry Chemical Physics*, 2015, **17**, 12957-12969.
6. X. Huang, *Journal of Power Sources*, 2014, **256**, 96-101.
7. P. Arora and Z. Zhang, *Chemical reviews*, 2004, **104**, 4419-4462.
8. T. Mayer-Gall, K. Opwis and J. S. Gutmann, *Journal of Materials Chemistry A*, 2015, **3**, 386-394.
9. J. H. Lin, M. C. Lin, A. P. Chen and C. W. Lou, *Advanced Materials Research*, 2014, **910**, 206-209.
10. H. Hori, U. Iwamoto, G. Niimi, M. Shinzato, Y. Hiki, Y. Tokushima, K. Kawaguchi, A. Ohashi, S. Nakai and M. Yasutake, *Journal of Artificial Organs*, 2015, **18**, 55-63.
11. X. Deng, A. Nikiforov, D. Vujosevic, V. Vuksanovic, B. Mugoša, U. Cvelbar, N. De Geyter, R. Morent and C. Leys, *Materials Letters*, 2015, **149**, 95-99.
12. B. O'regan and M. Grätzel, *Nature*, 1991, **353**, 737-740.
13. L. Tao, Z. Huo, Y. Ding, Y. Li, S. Dai, L. Wang, J. Zhu, X. Pan, B. Zhang, J. Yao, M. K. Nazeeruddin and M. Gratzel, *Journal of Materials Chemistry A*, 2015, **3**, 2344-2352.
14. S. B. Hong, S. H. Park, J. H. Kim, S. Y. Lee, Y. S. Kwon, T. Park, P. H. Kang and S. C. Hong, *Advanced Energy Materials*, 2014, **4**.
15. J. H. Kim, H. S. Jung, C. H. Park and T. J. Kang, *Journal of Physics and Chemistry of Solids*, 2014, **75**, 31-37.
16. A. Arof, M. Aziz, M. Noor, M. Careem, L. Bandara, C. Thotawatthage, W. Rupasinghe and M. Dissanayake, *international journal of hydrogen energy*, 2014, **39**, 2929-2935.
17. D. H. Lee, K. C. Sun, M. B. Qadir and S. H. Jeong, *Journal of nanoscience and nanotechnology*, 2014, **14**, 9377-9382.
18. X. Chen, J. Zhao, J. Zhang, L. Qiu, D. Xu, H. Zhang, X. Han, B. Sun, G. Fu and Y. Zhang, *Journal of Materials Chemistry*, 2012, **22**, 18018-18024.
19. D. R. MacFarlane, N. Tachikawa, M. Forsyth, J. M. Pringle, P. C. Howlett, G. D. Elliott, J. H. Davis, M. Watanabe, P. Simon and C. A. Angell, *Energy & Environmental Science*, 2014, **7**, 232-250.
20. P. Wang, S. M. Zakeeruddin, J. E. Moser, M. K. Nazeeruddin, T. Sekiguchi and M. Gratzel, *Nat Mater*, 2003, **2**, 402-407.
21. M. Dissanayake, C. Thotawatthage, G. Senadeera, T. Bandara, W. Jayasundera and B.-E. Mellander, *Journal of Photochemistry and Photobiology A: Chemistry*, 2012, **246**, 29-35.
22. N. Jeon, D. K. Hwang, Y. S. Kang, S. S. Im and D.-W. Kim, *Electrochemistry Communications*, 2013, **34**, 1-4.
23. Q. Li, H. Chen, L. Lin, P. Li, Y. Qin, M. Li, B. He, L. Chu and Q. Tang, *Journal of Materials Chemistry A*, 2013, **1**, 5326-5332.
24. R.-X. Dong, S.-Y. Shen, H.-W. Chen, C.-C. Wang, P.-T. Shih, C.-T. Liu, R. Vittal, J.-J. Lin and K.-C. Ho, *Journal of Materials Chemistry A*, 2013, **1**, 8471-8478.
25. D. Hwang, D. Y. Kim, S. M. Jo, V. Armel, D. R. MacFarlane, D. Kim and S.-Y. Jang, *Scientific Reports*, 2013, **3**, 3520.
26. S. H. Ahn, W. S. Chi, J. T. Park, J. K. Koh, D. K. Roh and J. H. Kim, *Advanced Materials*, 2012, **24**, 519-522.
27. K. Kakiage, Y. Aoyama, T. Yano, K. Oya, J.-i. Fujisawa and M. Hanaya, *Chemical Communications*, 2015, **51**, 15894-15897.
28. F. Bella, A. Lamberti, A. Sacco, S. Bianco, A. Chiodoni and R. Bongiovanni, *Journal of Membrane Science*, 2014, **470**, 125-131.
29. F. Bella, A. Chiappone, J. R. Nair, G. Meligrana and C. Gerbaldi, *Chemical Engineering Transactions*, 2014, **41**, 211-216.
30. W. Yi, Z. Huaiyu, H. Jian, L. Yun and Z. Shushu, *Journal of Power Sources*, 2009, **189**, 616-619.
31. A. Carbonell, T. Boronat, E. Fages, S. Girones, E. Sanchez-Zapata, J. A. Perez-Alvarez, L. Sanchez-Nacher and D. Garcia-Sanoguera, *Materials & Design*, 2015, **86**, 887-893.
32. Y. Li, L. Li, L. Cao and C. Yang, *Chemical Engineering Journal*, 2016, **283**, 1145-1153.
33. K. C. Sun, S. H. Yun, C. H. Yoon, H. H. Ko, S. Yi and S. H. Jeong, *Journal of nanoscience and nanotechnology*, 2013, **13**, 7938-7943.
34. M. B. Qadir, K. C. Sun, I. A. Sahito, A. A. Arbab, B. J. Choi, S. C. Yi and S. H. Jeong, *Solar Energy Materials and Solar Cells*, 2015, **140**, 141-149.
35. K. C. Sun, M. B. Qadir and S. H. Jeong, *RSC Advances*, 2014, **4**, 23223-23230.
36. P. K. Singh, K.-I. Kim, N.-G. Park and H.-W. Rhee, *Macromolecular Symposia*, 2007, **249-250**, 162-166.
37. A. A. Arbab, K. C. Sun, I. A. Sahito, M. B. Qadir and S. H. Jeong, *Applied Surface Science*, 2015.
38. Q. Wang, J.-E. Moser and M. Grätzel, *The Journal of Physical Chemistry B*, 2005, **109**, 14945-14953.
39. S. Zhang, X. Yang, C. Qin, Y. Numata and L. Han, *Journal of Materials Chemistry A*, 2014, **2**, 5167-5177.
40. M.-S. Kang, J. H. Kim, J. Won and Y. S. Kang, *The Journal of Physical Chemistry C*, 2007, **111**, 5222-5228.

41. J. Gao, M. B. Achari and L. Kloo, *Chemical Communications*, 2014, **50**, 6249-6251.
42. N. Inagaki, S. Tasaka, K. Narushima and H. Kobayashi, *Journal of Applied Polymer Science*, 2002, **85**, 2845-2852.